SnO$_2$:Sb transparent conducting coatings made by different sol-gel processes

G. Gasparro, D. Ganz, C. Göbbert, J. Pütz, M. A. Aegerter

Institut für Neue Materialien - INM, Im Stadtwald, Gebäude 43, 66123 Saarbrücken, Germany

ABSTRACT

Single and multilayer sol-gel coatings of transparent antimony-doped tin oxide (SnO$_2$:Sb) have been prepared on borosilicate and fused silica substrates using either a 5 mole% SbCl$_3$ doped 0.5 M solution of SnCl$_2$(OAc)$_2$ in ethanol or a water suspension of crystalline Sb-doped tin oxide nanoparticles. The nanoscale morphology and the electrical parameters of the layers have been determined after different firing procedures and heating rates varying from 0.2 to 4300 K/s obtained either in a furnace or by cw CO$_2$ laser irradiation. For a given sintering temperature (~540°C) a slow heating process in furnace leads to porous, homogeneous single and multilayers consisting of small crystallites. They present a high resistivity of about $\rho = 4 \times 10^{-2}$ Ωcm. With increasing heating rate the layers become denser with larger crystallites and the resistivity value decrease down to ~ 7×10^{-3} Ωcm for 4300 K/s (CO$_2$ laser sintering). It is proposed that the densification of the coatings is determined by a competition between nucleation at low temperatures and the growth of the crystallites at high temperatures.

Keywords: Sol-gel, thin film, electronic conductor, SnO$_2$:Sb, morphology, structure, electrical parameters, heating rate

1. INTRODUCTION

Transparent electrically conducting coatings (TEC) on glass are used today in a wide range of optoelectronic applications [1, 2]. The materials which present the most interesting properties are n-type semiconductors such as indium tin oxide (ITO), fluorine or antimony doped tin dioxide (FTO, ATO), and zinc oxide (ZO) doped with Al (AZO) and Ga (GZO). Practically all known coating processes have been used to deposit them [1]. Transparent ITO and FTO coatings prepared by sputtering and spray pyrolysis techniques, respectively, are available commercially with resistivities as low as 2×10^{-4} Ωcm.

The sol-gel process [3] has been successfully applied for the obtention of ITO coatings [4-9]. Their electrical and optical properties are strongly dependent on the nature of the solutions and the temperature and atmosphere used during the sintering process. The lowest resistivities have always been obtained after sintering at relatively high temperatures (600°C or higher) and the best published value, $\rho = 1.8 \times 10^{-4}$ Ωcm [7], is comparable to those typically obtained by other processes.

Few research has been addressed to the preparation of sol-gel antimony doped tin dioxide (ATO) coatings. Most of the sols have been prepared from Sn(IV)-alkoxides such as Sn-ethoxide [10-12], Sn-propoxide [5, 13], Sn-butoxide [14-16] or more complex systems [15-18]. SnCl$_4$ [15, 16, 19, 20], SnCl$_2$ [15, 16], Sn(II)-2-ethylhexanoate [15, 16, 21], and Sn(II)-citrate [22] have also been used. Antimony doping is usually obtained by addition of SbCl$_3$ [19, 23, 24], Sb(OEt)$_3$ [11-13, 15, 16] or Sb(OBu)$_3$ [5, 17, 21], whereas fluorine doping has not yet been achieved by the sol-gel process. The use of sol stabilisers is only reported for a few solutions [13, 15, 16, 22].

SnO$_2$:Sb sol-gel coatings obtained until now present a relatively high resistivity, the lowest published value of $\rho = 3 \times 10^{-3}$ Ωcm [12], exceeding by more than one order of magnitude those obtained for coatings prepared by other methods (e.g. $\rho = 1 \times 10^{-5}$ Ωcm for Activated Reactive Evaporation of SnO$_2$ and SnO$_2$:Sb [25].

Further author information:
M. A. Aegerter (correspondence):   e-mail: aegerter@inm-gmbh.de, Tel.:+49-+681-302 5017, Fax:+49-+681-302 5249

The reasons for which highly conductive SnO_2:Sb films cannot be obtained by the sol-gel process are still not clear. The influence of the chemical composition of the sol on the resistivity of the coatings has been studied in detail by Pütz et al. [15, 16] using different precursors such as $Sn(OtBu)_4$, $SnCl_4$, $SnCl_2(OAc)_2$, $Sn(OAc)_4$, $SnCl_2$, and Sn-(II)-2-ethylhexanoate and stabilisers such L(+)-tartaric acid, succinic acid, citric acid, oxalic acid, triethanolamine, ethylenediamine, acetylacetone and diacetone alcohol and 5 mole% $SbCl_3$ as dopant. The conductivitiy of the coatings were found strongly dependent on the type of precursor.

The use of an adequate stabiliser was found essential for $SnCl_4$-based solutions as the high chloride content of the solution leads to both volatile antimony and tin compounds which are lost during the early stages of the firing process [15, 26]. On the other hand, the stabilisers have little influence in alkoxide-based sols which have to be stabilised only against uncontrolled hydrolysis [15, 27]. Chatelon et al. [11] observed a minimum in the film resistivity when the dip coating procedure was performed in an atmosphere of 30 - 40% RH. The resistivity increases drastically when alkaline impurities are present in the coating and SiO_2 [28] or TiO_2 [13, 28] buffer layers are necessary when alkaline glass substrates are used. Another important factor is the coating microstructure which consists of small, almost spherical grains aggregated in a rather loose packed structure even after calcination at temperature as high as 800°C [13, 16, 29-31]. For pure SnO_2 coatings the grain growth is suppressed and the grain size increases with the film thickness [31].

This paper presents experimental results obtained recently at INM on single and multilayer sol-gel SnO_2:Sb coatings prepared by various sols, deposition procedures and sintering processes in which the heating rates are varied over a large scale (0.2 to 4300 K/s) and discusses their influence on the coating morphology and the resulting electrical parameters.

2. EXPERIMENTAL

Single and multilayer sol-gel coatings have been deposited using a 0.5 M ethanolic solution of $SnCl_2(OAc)_2$ containing 5 mole% $SbCl_3$ by dip coating technique with a withdrawal speed of 2 to 10 mm/s on borosilicate or fused silica substrates in a controlled atmosphere (40% RH, 20°C). The particular choice of this sol was based on factors such as cost of the precursors, easiness of preparation, or chemical stability, although it was not the preparation which allows the obtention of coatings with the lowest resistivity [15, 16]. The same sol was also used to obtain coatings by spray pyrolysis at $T \cong 500°C$. Crystalline SnO_2:Sb nanoparticles with a 3 to 5 nm average size prepared by a hydrothermal process and redispersed in water or a stabilised tin(II)-chloride ethanolic sol [32] have also been used to prepare single or multilayers by spin coating technique under the same conditions. The sintering was performed in air after drying the layer at room temperature or higher temperature with heating rates varying from 0.2 to 4300 K/s using either conventional furnace heating or cw CO_2 laser irradiation whose set up is described elsewhere [33, 34]. Figure 1 shows a flow diagram of the different procedures. The thickness of the coating was measured with a surface profiler (Tencor P 10). Their structure has been determined by X-ray diffraction (XRD) at glancing incidence using a Siemens D500 instrument, their density by Rutherford back scattering (RBS). Their texture has been observed by high resolution transmission electron microscopy (HRTEM Philips CM 200 FEG) and the surface morphology by scanning electron microscopy (SEM) with a JEOL 6400 F instrument. The electrical properties of the coatings have been determined by 4 probes and by van der Pauw/Hall technique [35, 36] (MMR Technology with a 1.5 T magnetic field).

3. RESULTS AND DISCUSSION

3.1 Influence of the substrate

The room temperature resistivity ρ of 90 to 105 nm thick SnO_2:Sb single layers processed according to procedure II (Fig. 1) is shown in figure 2. For coatings deposited on fused silica substrates, ρ gradually decreases with increasing temperature down to a minimum of 9×10^{-3} Ωcm (sheet resistance $R_\square = 900$ $\Omega_\square$) at $T \cong 700°C$. The increase observed with a borosilicate glass substrate at temperatures above 550°C is probably due to the onset of Na^+ diffusion from the substrate into the layer.

The sintering temperature is therefore an important parameter but even at quite high temperature ($T \cong 700°C$) the resistivity of the coatings is still about a factor ten higher than those obtained by other deposition processes.
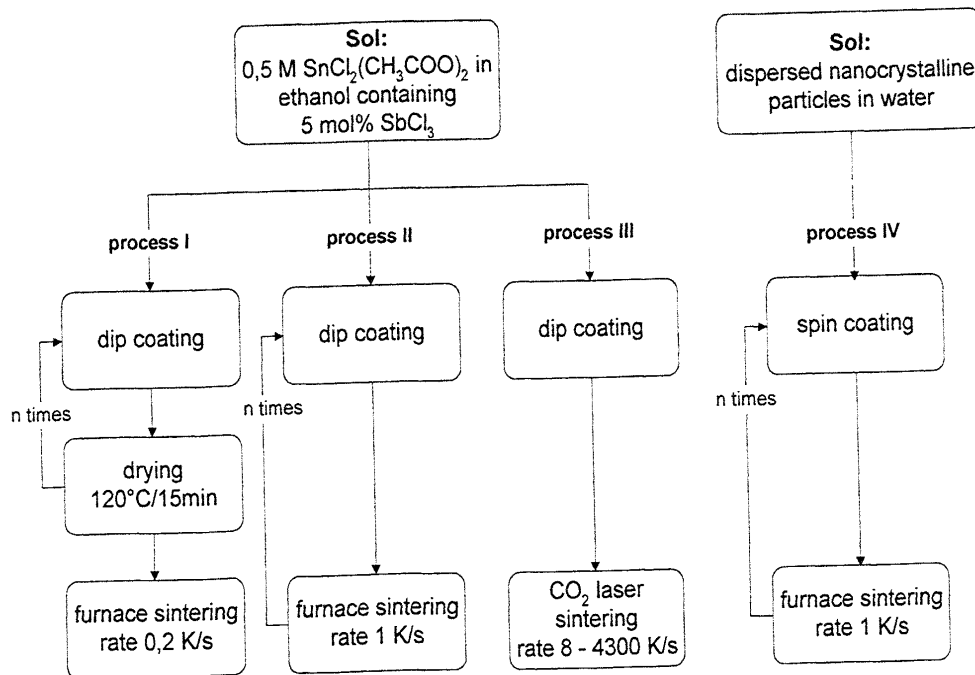
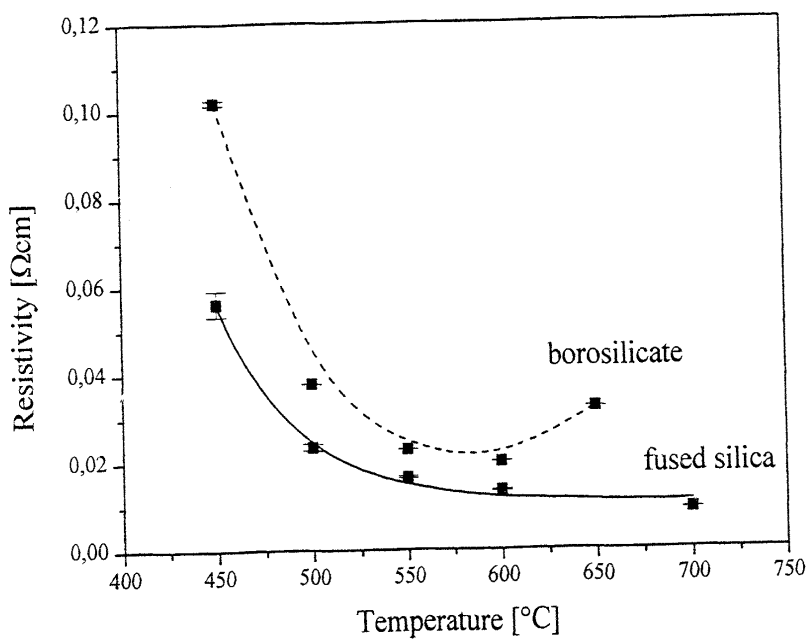Fig. 1: Flow diagram of the different procedures.

Fig. 2: Room temperature resistivity vs. sintering temperature for single SnO_2:Sb layers of about 100 nm thickness dip coated on borosilicate glass and fused silica substrates. The error bars give the standard deviation of the mean of 12 measurements. The lines are drawn as guides for the eye.

3.2 Influence of the sintering process

An important factor was discovered by studying the morphology of the coatings prepared under different deposition and heating conditions. Coatings prepared by spray pyrolysis consist of large crystallites densely packed in a columnar structure

of cassiterite type (Fig. 3). Single and multilayer coatings prepared by dip coating according to process I involving a drying process at 120°C are composed of small (6 to 8 nm) almost spherical crystallites (untextured cassiterite structure) that are loosely packed. The layer is porous and its top surface is smooth (Fig. 4). On the contrary, the morphology of single and multilayers coatings obtained according to process II, (firing in a preheated furnace without predrying), reveals that each individual layer consists of a thin (< 10 nm), relatively dense interface (external part) lying on top of a more porous material (internal part) (Fig. 5) [33, 34, 37]. The morphology of single layers sintered by means of a slow scan cw CO_2 laser irradiation (process III), shows that such layers are still made of untextured crystallites which are, however, slightly larger and packed in a denser structure (Fig. 6). Finally, the morphology of single and multilayer coatings made with the sol prepared with a sol containing small crystalline nanoparticles (process IV) resembles to the morphology obtained by process II, i.e. each layer presents a thin and dense top layer on a porous internal part. The layers are also composed of small crystallites (Fig. 7).

These different morphologies have a drastic effect on the electrical parameters of the coatings. The resistivity of multilayer coatings prepared by process I is practically independent of the layer thickness as the complete coating is homogeneous. The sheet resistance thus is inversely proportional to the thickness. The corresponding resistivity is $\rho \sim 1.5 \times 10^{-2}$ Ωcm. The resistivity of coatings prepared according to process II and IV is strongly dependent of the coating thickness and the thickness of the top layer interface. For the same total thickness, the resistivity was found to decrease with an increased number of layers, as the fraction of denser material in the film becomes larger. It was shown [38] that multilayer coatings can be described as a sequence of thick layer having a high resistivity of $\rho_i \cong 200$ Ωcm (internal part of each layers), and a thin layer having a low resistivity $\rho_e \cong 1.8 \times 10^{-3}$ Ωcm, with all layers being electrically connected in parallel.

The lowest resistivity of laser sintered single layers so far obtained is $\rho \cong 3.2 \times 10^{-3}$ Ωcm.

3.3 Influence of the heating rate

The above experiments have shown that the sintering procedure of SnO_2:Sb films has a drastic influence on their microstructure and resistivity. It is shown below that, in fact, the initial heating rate has a substantial influence on their microstructure and thus determines the electrical properties of the coatings. The following tests have been done on a series of dip coated single layer samples having the same initial thickness of the dried gel film of 158 nm. They have then been sintered at T = 540°C with different heating rates which have been varied over a large scale from 0.2 to 4300 K/s, using either a furnace (slow heating, 0.2 K/s, and heating in a preheated furnace, 1 to 2 K/s) or a large and a small spot cw CO_2 laser irradiation, 8 to 4300 K/s [37]. After the initial heating ramp the sintering temperature was kept constant for a period of up to 1000 s.

The variation of the sheet resistance with the heating rate is given in figure 8 where the first values in each series corresponds to the ramp time τ_r. The sheet resistance decreases with increasing heating rate from about 5 k$\Omega_\square$ (0.2 K/s) to 800 $\Omega_\square$ (4300 K/s). The influence of the sintering time τ_S on the sheet resistance represented by the following values in each series depends on the heating rates. For high heating rates of 100 to 500 K/s the sheet resistance stays nearly constant in time whereas the sheet resistance for furnace fired samples with a heating rate of 0.2 K/s slightly decreases by a factor 1.5. The final sheet resistance is dependent as well on the heating rate.
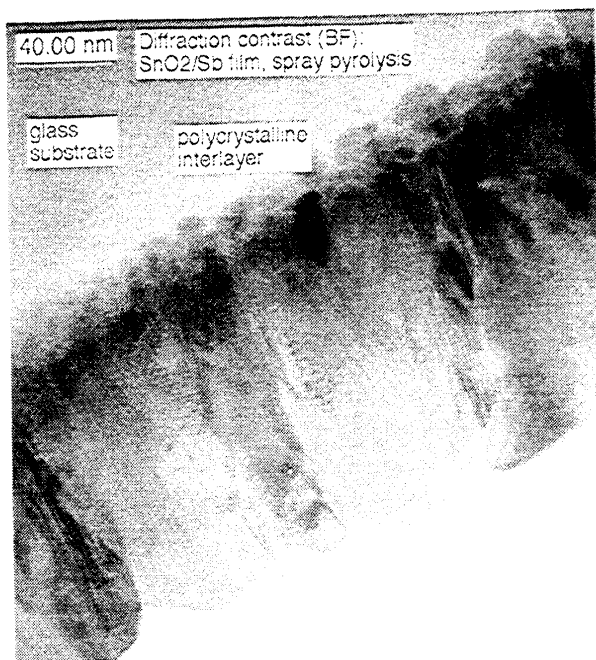
Fig. 3: TEM cross-section of a 177 nm thick spray pyrolysed SnO$_2$:Sb coating
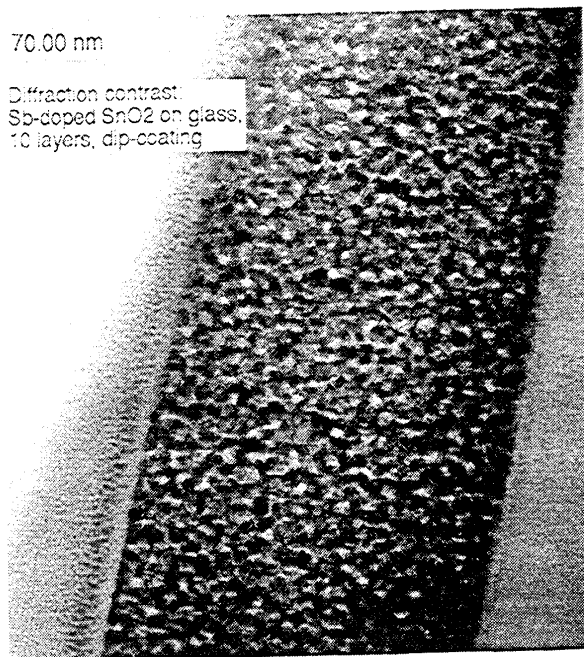

Fig. 4: HRTEM cross section of a 10 layers coating (thickness ~ 290 nm) prepared according to process I
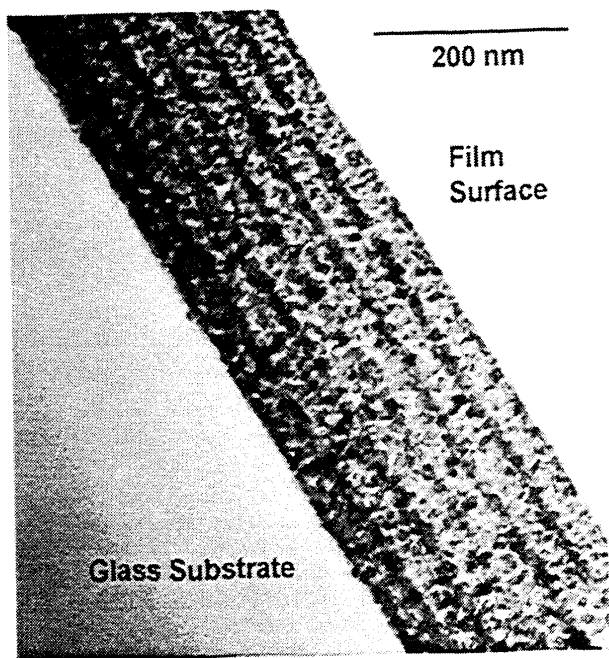

Fig. 5: HRTEM cross section of a 10 layers coating (thickness ~ 290 nm) prepared according to process II
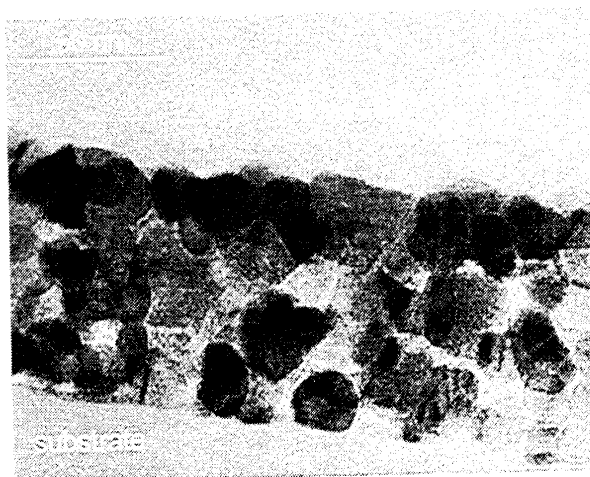

Fig. 6: HRTEM cross section of a single layer sintered by CO$_2$ laser irradiation at T = 550°C, thickness ~ 80 nm (process III)

70.00 nm   Diffraction contrast:
           Sb-doped SnO2/glass,
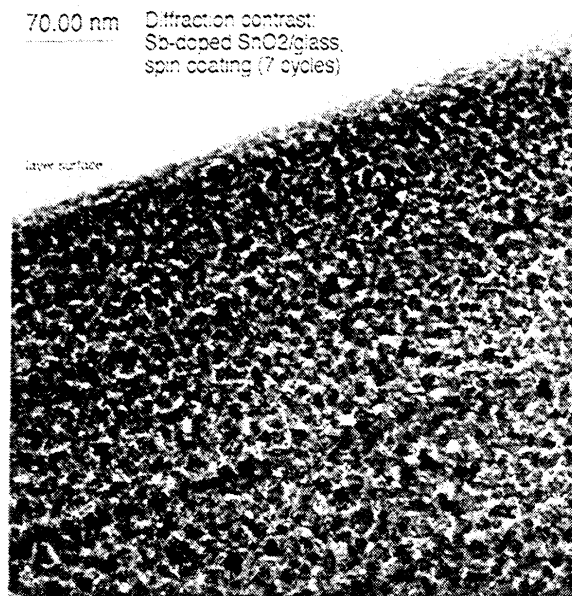   spin coating (7 cycles)

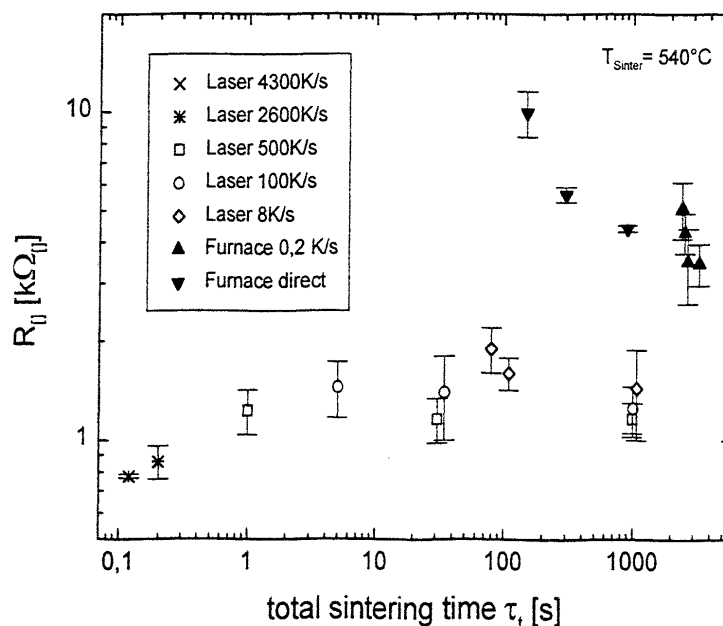Fig. 7: HRTEM cross section of a multilayer coating prepared according to process IV at 550 °C.

Fig. 8: Sheet resistance of SnO_2:Sb coatings prepared with different heating rates using either a furnace or a cw CO_2 laser at a final sintering temperature of 540°C

These variations in sheet resistance cannot be attributed to a change in film thickness as can be seen from figure 9 but should rather come from differences in the microstructure of the coatings. The initial thickness of the gel film of 158 nm is reduced to about 140 nm at a heating rate of 0.2 K/s in the furnace and to 107 nm for the laser treated sample with 4300 K/s. The furnace samples show a shrinkage of less than 10% indicating that the porous structure of the gel film is mainly retained while the laser treated samples with a higher shrinkage of about 30% should have a denser structure. As the total mass of the films has to be the same, this can only reflect a large difference in film density which has been proved by

RBS density measurements. The densities thus obtained are 3.2 g·cm^{-3} and 4.8 g·cm^{-3} for the furnace and laser treated sample, respectively, which corresponds to a porosity of 50% and 30% with a theoretical density of 7.0 g·cm^{-3} for pure SnO_2.
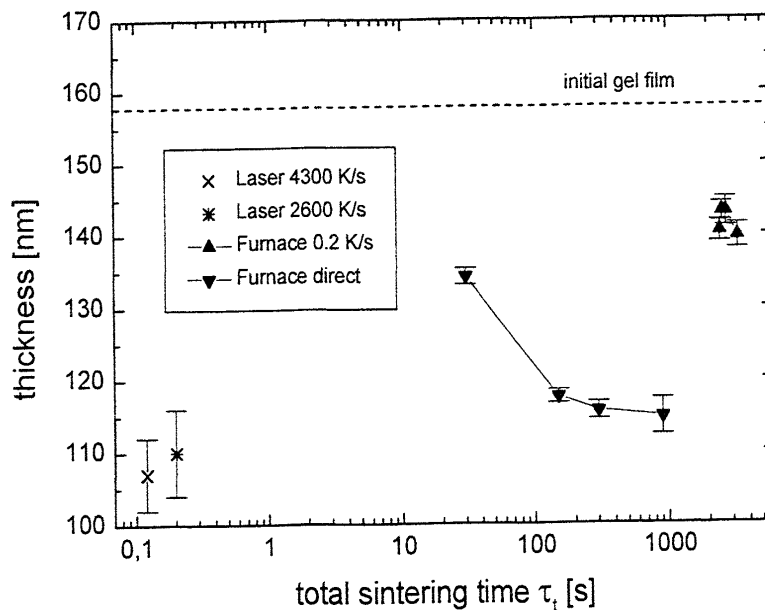

Fig. 9: Film thickness of samples heat treated with different heating rates at a final sintering temperature of 540°C. The thickness of the initial gel film is 158 nm

This difference in morphology is clearly seen in the HRTEM cross-sections of samples heat treated at the same temperature of 540°C in a furnace and by laser irradiation, respectively (Fig. 4 and 6).

A similar trend of densification with increasing heating rate is evidenced by the crystallographic grain size. The furnace samples typically have crystallite sizes of 5-6 nm whereas higher heating rates lead to crystallite sizes of 8 nm (2600 K/s) and 12 nm (4300 K/s) for final temperatures of 540°C.

These results lead to the conclusion that a competition between nucleation and crystal growth is responsible for the differences in the densities. At lower temperatures a nucleation process takes place whereas at higher temperatures a growth of the crystallites can be observed [39]. Low heating rates favour the formation of numerous nuclei. By the use of high heating rates this nucleation process is passed through very quickly leading to few nuclei that can grow more easily as the diffusion ways are shorter.

The series of directly furnace fired samples shows a different behaviour with a higher decrease in sheet resistance from 800 kΩ$_\square$ to 4.4 kΩ$_\square$ after 15 min (Fig. 8). The final thickness of the film of 115 nm (Fig. 9) is smaller than that of the slowly heated furnace samples but only slightly higher than that obtained with laser treated samples. This higher densification in direct furnace firing compared to slowly furnace fired films comes from the formation of a dense top layer, which is shown in figure 5.

An explanation for this could be different mechanisms of heating for direct and slow furnace firing, respectively, and for CO_2 laser treatment. For the low heating rates in the furnace a uniform temperature profile through the sample can be assumed. The slow increase in temperature allows for a complete escape of volatile compounds during film formation. The structure of the coatings is homogeneous and porous, reflecting the loose structure of the gel film. The film is formed by the aggregation of small crystallites which results in a high sheet resistance due to a large number of grain boundaries. In direct furnace firing the heat transport has to be accomplished from the film surface to the substrate. The upper film surface is heated quickly leading to a thin dense layer which seals the film bulk. Thus, the evaporation of residues from the gel film is impeded and a further heating is retarded as the formed conductive coating reflects heat radiation and the sample is heated mainly by heat conduction. Due to this retarded heating the heating rates for the bulk of the film and the substrate should be in the order of 1 K/s indicated by the lower limit in film thickness. As a consequence the film's bulk exhibits a structure
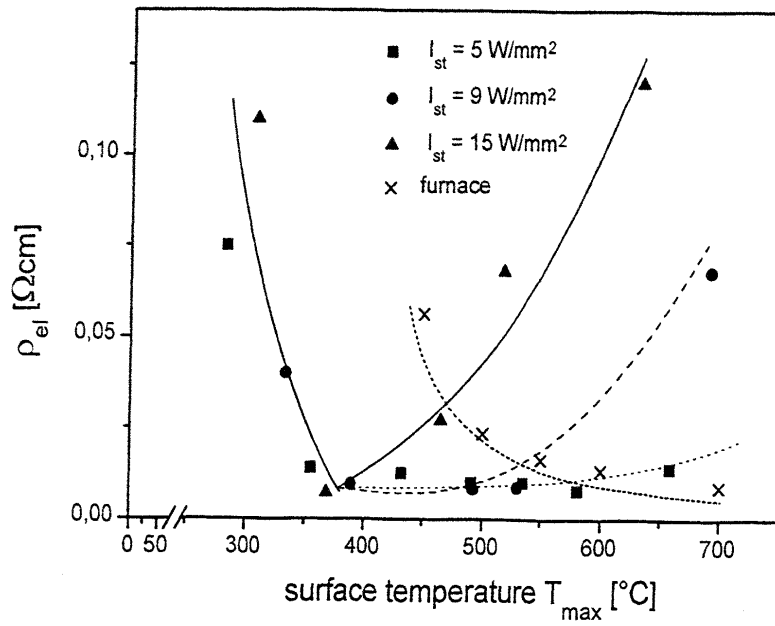
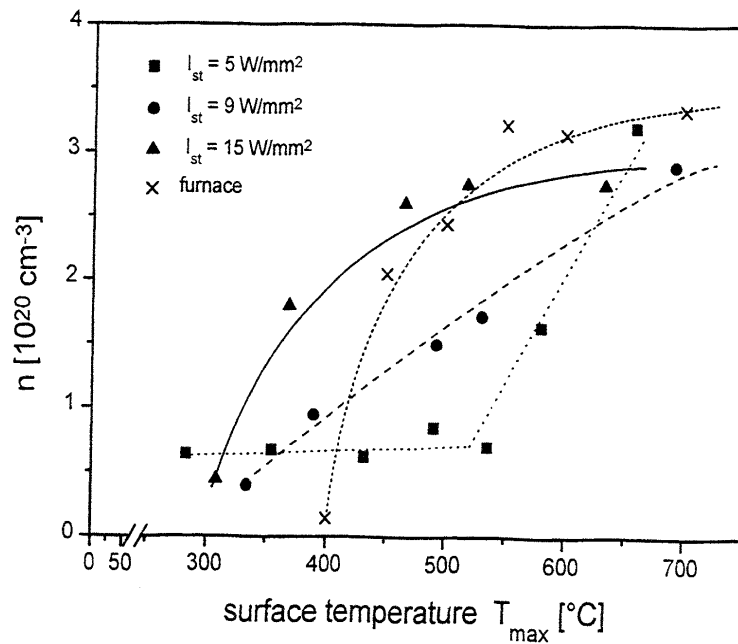Fig. 10: Variation of the resistivity ρ vs. the sintering temperature. The lines drawn are guides for the eye

Fig. 11: Variation of the carrier density n vs. the sintering temperature. The lines drawn are guides for the eye

similar to that observed with slow furnace firing. The sheet resistance in both films is about the same as the crystallite sizes are similar, but for the directly furnace fired sample this is obtained with a lower film thickness. This implies a higher overall density for these films.

In contrast, the laser treated samples are mainly heated from the substrate side as the gel film practically does not absorb at 10.6 μm. The sintering of the films proceeds from the substrate towards the film surface. As the transport of heat through the thin film is fast and hence the heating is high, the low number of nuclei that is formed in this time allows a growth of larger crystallites. This leads to a homogeneous structure with a higher density and consequently to a better sheet resistance due to a reduced number of grain boundaries.

3.4 Influence of the temperature

As already discussed above, the resistivity of SnO_2:Sb coatings deposited on fused silica substrates and heat treated in a furnace decreases with the sintering temperature and reaches its lowest value at high temperatures ($\sim$ 800°C). A comparison of the electrical parameters (resistivity ρ, mobility μ, carrier density n) measured as a function of the sintering temperature is now presented for single layer coatings sintered by high power fast scan CO_2 irradiation (process III, heating rate up to 7000 K/s) [33, 34, 40] and furnace firing (process II, heating rate $\sim$ 1 K/s).

The resistivity is depicted in figure 10 as a function of the maximum temperature achieved. It decreases with increasing temperature for all laser power densities until $\approx$ 400°C and then increases rapidly at higher temperatures with a slope that increases with the power density. For laser power density $I_{st} = 5$ W/mm^2 the resistivity reaches a minimum value $\rho \approx 8 \times 10^{-3}$ Ωcm at about 500°C. For $I_{st} = 15$ W/mm^2 the minimum is $\rho \approx 6.8 \times 10^{-3}$ Ωcm and lies at $T_{max} = 375$°C. The corresponding resistivity of the furnace fired coatings gradually decreases with temperature to a minimum value $\rho = 9 \times 10^{-3}$ Ωcm at 700°C (Fig. 10).

This behavior can be understood by analyzing the temperature dependence of the carrier density n and the electron mobility μ. The carrier density increases monotonically with T_{max} (Fig. 11) and saturates at a temperature of 600°C at a value $n \approx 3 \times 10^{20}$ cm^{-3} for all heat treatment processes. For the laser treated samples the slope of the curves is the steeper the higher the power density is. As the temperature increases the network formation due to chemical reactions occurring in the coatings increases which leads to an increase of the carrier concentration. However at 600°C all chemical reactions are completed so that the carrier density can not be increased any longer and reaches a maximum value ($n \approx 3 \times 10^{20}$ cm^{-3}).

The electron mobility (Fig. 12) shows a complementary behavior to that of the resistivity. It increases with increasing temperature for all laser power densities up to a certain temperature and then decreases separately for each power density. This decrease is the faster the higher the power density is. Each curve has a maximum at a different temperature. The behavior of μ for the samples heat treated in a furnace is different. The overall values are smaller and increase only slightly with the temperature.

The fact that the electron mobilities of all laser fired samples follow the same temperature dependence up to ca. 420°C is essentially due to the network formation. At higher temperatures the crystallite size starts to increase leading to an increase in the mobility (Fig. 13)

The individual decrease for each power density is due to the formation of cracks by strong temperature gradients. These cracks do not appear in furnace fired samples. The difference in the temperature dependence of the laser and furnace fired samples can be understood in terms of densification and crystal growth. The high heating rates (up to 7000 K/s) during laser firing cause a densification rather than a nucleation of the films. The films are highly densified with a small amount of nuclei. These nuclei grow larger as the temperature rises and the morphology of the layer is formed by large and densely packed crystallites (Fig. 6). This leads to a high electron mobility in the laser fired samples. In a furnace the coatings are fired at a low heating rate. This creates many nuclei and no significant densification. With rising temperature this large amount of nuclei grows slightly resulting in a porous layer composed of small crystallites.
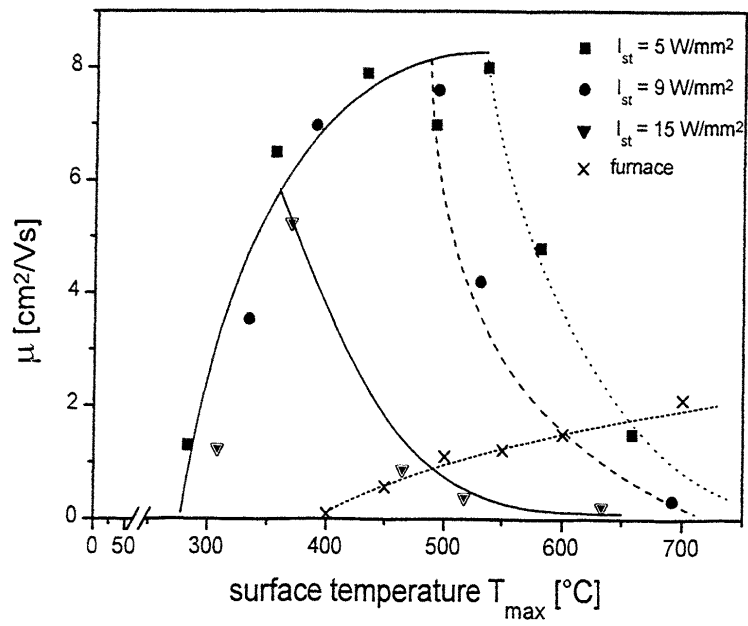
Fig. 12: Variation of the electron mobility μ vs. the sintering temperature. The lines drawn are guides for the eye
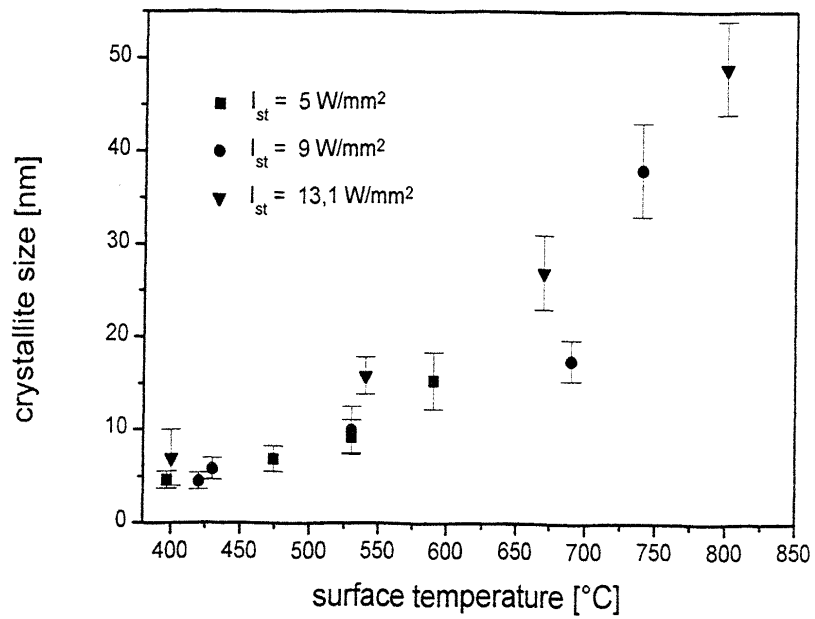

Fig. 13: Temperature dependence of the crystallite size

CONCLUSION

Heat treatment procedures, heating rates and sintering temperature influence drastically the morphology and the electrical parameters of dip and spin coated sol-gel SnO_2:Sb coatings. At sintering temperatures between 350 and 800°C, their coatings morphology always consists of almost spherical crystallites of cassiterite structure, whatever the sintering procedure used (furnace or cw CO_2 laser irradiation).

For single layers and a given sintering temperature (exemplified here for T = 540°C), the size of the crystallites and the density of the layers increase with the heating rate. These variations are correlated to a decrease of the resistivity and sheet resistance from 4.4 $k\Omega_\square$ for a 0.2 K/s heating rate down to ~ 800 $\Omega_\square$ for a rate of 4300 K/s. It is proposed that this is caused by a competition between nucleation at low temperatures and the growth of the nuclei occurring at higher temperatures. A low heating rate (~ 0.2 K/s), as obtained in a conventional furnace, leads to a low densification and favors consequently a porous structure of small crystallites. High heating rates, larger than 8 K/s which can be obtained by high power CO_2 laser irradiation favor a denser structure built with larger crystallites and fewer pores. The porosity and the limited crystallite size of sol-gel processed SnO_2:Sb coatings can therefore be overcome by application of high heating rates. A 100 nm thick coating presenting a resistivity as low as 3×10^{-3} Ωcm (sheet resistance of 250 $\Omega_\square$) [40] has been obtained using this process.

Multilayer coatings processed at a slow heating rate are homogeneous but their resistivity is high ($\rho \cong 1$ to 4×10^{-2} Ωcm) and practically independent of the thickness. Their morphology is similar to that of single coatings. Coatings sintered in a preheated furnace at a higher rate (~ 1 to 2 K/s) exhibit an inhomogeneous structure. Each film is composed of a thin (< 10 nm) dense external layer on top of a porous thick structure. The thin interface layer has a much smaller resistivity than the bulk of the film. Multilayers are built of a sequence of such layers and the overall resistivity of the final coating decreases with the number of layers. A resisivity as low as 3.5×10^{-3} Ωcm (sheet resistance of 120 $\Omega_\square$) has been obtained with a 290 nm thick 10-layer coating.

Coatings made with 3 to 5 nm sized crystalline nanoparticles present the same feature. The final resistivity of these coatings is not improved as in the dry state, before sintering, they already present a high number of small nuclei which are impeded to grow. In order to take advantage of this preparation technique, larger nanocrystalline particles have to be synthesised. In this way, the crystal growth process will be transferred to a wet chemical process.

From the experimental point of view, it is also worth mentioning that CO_2 laser firing, which allows to heat glass substrates directly, appears as an interesting technique for the investigation of sintering processes of coatings with a variable heating rate from 0.1 up to ~ 10^4 K/s.

417

REFERENCES

1. K. L. Chopra, S. Major, D. K. Pandya, Thin Solid Films **102**, 1 (1983)
2. C. G. Granqvist, Thin Solid Films **193/194**, 730 (1990)
3. C. J. Brinker and G. Scherer, „Sol-Gel Science", Acad. Press Ltd., San Diego (1990)
4. N. J. Arfsten, R. Kaufmann, H. Dislich, German Patent DE 3300589 A 1 (1984)
5. M. Mattox, Thin Solid Films **204**, 25 (1991)
6. T. Furusaki, K. Kodaira, in: „High Performance Ceramic Films and Coatings", P. Vincenzini (ed.), 241, Elsevier Science Publishers (1991)
7. O. Yamamoto, T. Sasamoto, M. Inagaki, J. Mater. Res. **7**, 2488 (1992)
8. Y. Takahashi, H. Hayashi, Y. Ohya, Mater. Res. Soc. Symp. Proc. **271**, 401 (1992)
9. K. Nishio, T. Sei, T. Tsuchiya, J. Mater. Sci. **31**, 1761 (1996)
10. A. Maddalena, R. Del Machio, S. Diré, A. Raccanelli, J. Non-Cryst. Solids **121**, 365 (1990)
11. J. P. Chatelon, C. Terrier, E. Bernstein, R. Berjoan, J. A. Roger, Thin Solid Films **247**, 162 (1994)
12. C. Terrier, J. P. Chatelon, R. Berjoan, J. A. Roger, Thin Solid Films **263**, 37 (1995)
13. Y. Takahashi, Y. Wada, J. Electrochem. Soc. **137**, 267 (1990)
14. J. C. Giuntini, W. Granier, J. V. Zanchetta, A. Taha, J. Mater. Sci. Lett. **9**, 1383 (1990)
15. J. Pütz, Diploma Thesis, Universität des Saarlandes, Saarbrücken, Germany (1996)
16. G. Gasparro, J. Pütz, D. Ganz, M. A. Aegerter, Proceedings Eurosun´96, Freiburg, Germany, 17-19.09.1996, to appear in Solar Energy Materials And Solar Cells (1997)
17. J. R. Gonzales-Oliver, I. Kato, J. Non-Cryst. Solids **82**, 400 (1986)
18. S.-S. Park, J. D. Mackenzie, Thin Solid Films **258**, 268 (1995)
19. D. E. Stilwell, S.-M. Park, J. Electrochem. Soc. **129**, 1501 (1982)
20. R. S. Hiratsuka, S. H. Pulcinelli, C. V. Santilli, J. Non-Cryst. Solids **121**, 76 (1990)
21. A. Tsunashima, H. Yoshimizu, K. Kodaira, S. Shimada, T. Matsushita, J. Mater. Sci. **21**, 2731 (1986)
22. P. Olivi, E. C. Pereira, E. Longo, J. A. Varella, L. O. S. Bulhoes, J. Electrochem. Soc. **140**, L 81 (1993)
23. G. Gowda, D. Nguyen, Thin Solid Films **136**, L 39 (1986)
24. B. Orel, U. Lavrencic-Stangar, Z. Crujak-Orel, P. Bukovec, M. Kosec, J. Non-Cryst. Solids **167**, 272 (1994)
25. H. S. Randhawa, M. D. Matthews, R. F. Bunshah, Thin Solid Films **83**, 267 (1981)
26. D. C. Bradley, E. V. Caldwell, W. Wardlaw, J. Chem. Soc. **1957**, 3039
27. M. J. Hampden-Smith, T. A. Wark, C. J. Brinker, Coord. Chem. Rev. **112**, 81 (1992)
28. W. Lada, A. Deptula, T. Olczak, W. Torbicz, D. Pijanowska, J. Sol-Gel Sci. Tech. **2**, 551 (1994)
29. M. Kanamori, M. Takeuchi, Y. Ohya, Y. Takahashi, Chem. Lett. **2035** (1994)
30. D. J. Yoo, J. Tamaki, N. Miura, S. J. Park, N. Yamazoe, J. Electrochem. Soc. **142**, L105 (1995)
31. D. J. Yoo, J. Tamaki, S. J. Park, N. Miura, N. Yamazoe, J. Am. Ceram. Soc. **79**, 2201 (1996)
32. D. Burgard, C. Göbbert, R. Nass, Proc. Int. Workshop Sol-Gel '97, 31.08-05.09.97, Sheffield, UK (submitted)
33. D. Ganz, G. Gasparro, J. Otto, A. Reich, N. J. Arfsten, M. A. Aegerter, J. Mater. Sci. Lett. **16**, 1233 (1997)
34. D. Ganz, A. Reich, M. A. Aegerter, J. Non-Cryst. Solids, to be published (1997)
35. L. J. Van der Pauw, Philips Res. Rep. **13**, 1 (1958)
36. A. A. Ramadan, R. D. Gould, A. Ashour, Thin Solid Films **239**, 272 (1994)
37. D. Ganz, M: A. Aegerter, Proc. Int. Workshop Sol-Gel '97, 31.08-05.09.1997, Sheffield, UK (submitted)
38. J. Pütz, D. Ganz, G. Gasparro, M. A. Aegerter, Proc. Int. Conference, Sol-Gel '97, 31.08-05.09.1997, Sheffield, UK (submitted)
39. M. Avrami, J. Chem. Phys. **9**, 177 (1941)
40. G. Gasparro, D. Ganz, J. Pütz, M. A. Aegerter, J. Non-Cryst. Solids, to be published (1997)